Acta Cryst. (1997). B53, 143–152

4*f*-Electron Density Distribution in Crystals of CeB_6 at 165 K and its Analysis Based on the Crystal Field Theory

KIYOAKI TANAKA,[a]* YOSHIO KATO[a] AND YOSHICHIKA ŌNUKI[b]

[a]*Chemistry Department, Nagoya Institute of Technology, Gokiso-cho, Showa-ku, Nagoya 466, Japan, and* [b]*Physics Department, Osaka University, Machikaneyama-cho, Toyonaka 560, Japan. E-mail: kiyo@tana1.kyy.nitech.ac.jp*

(Received 26 March 1996; accepted 3 July 1996)

Abstract

4*f*-Electron density in single crystals of CeB_6, cerium hexaboride, was measured at 165 K by X-ray diffractometry. Significant peaks 2.0 e Å^{-3} high were found along the ⟨100⟩ directions at 0.41 Å from Ce on the deformation density map. Analysis based on the crystal field theory removed the peaks, confirming that they were due to the Ce 4*f*-electrons on the t_{1u}-orbital. The deformation density in the B_6 octahedron was also markedly improved by the analysis and coincides qualitatively with a theoretical molecular orbital (MO) calculation. It also coincides with the model deformation density map of CaB_6 composed of only light atoms. These facts guarantee the accuracy of the intensity measurement for the present study. Since Ce^{3+} has only one 4*f*-electron, a highly accurate intensity measurement is necessary to detect its 4*f*-electron density distribution. A ψ-scan technique was therefore employed to avoid multiple diffraction (MD) and to measure the intensities at ω and χ angles with minimum fluctuation of temperature at the sample position. Relativistic radial functions for orbitals of Ce^{3+} and the corresponding scattering factors, which take the aspherical electron density distribution of 4*f*-electrons into account, were used for the analysis. CeB_6 is a typical dense Kondo material. The Kondo effect occurs in CeB_6 from low temperature to above room temperature. X-ray analysis of the *f*-electron density based on atomic orbitals (AO) revealed that 1.5 (2) electrons are donated from B_6 to Ce and a total of 2.5 (2) electrons localize on the 4*f*-orbital. κ values are consistent with the 4*f*-orbitals being highly contracted and thus stabilized. These may be related to the Kondo effect.

1. Introduction

Some rare-earth compounds have excellent properties as magnets, photoemission substances for lasers, phosphorescence materials, hydrogen-absorbing alloys, and so on. Some were recently shown to be excellent catalysts for stereospecific polymerizations. Rare-earth elements are also involved in high-temperature superconductors. These characteristics of rare-earth compounds are correlated to the *f*-electrons. However, measurement of the *f*-electron density has been considered difficult for the following three reasons. First, the 4*f*-orbitals are shielded by fully occupied 5*s*- and 5*p*-shells, which are located outside the *f*-orbitals. Differentiating the 4*f*-electron density from those of the outer lying orbitals had been considered difficult. In addition, since the aspherical electron density is due to the combined effect of the aspherical electron configuration and thermal vibration of the nucleus, distinguishing the two effects appears to be very difficult, especially for the inner-lying 4*f*-electrons. Second, the small ratio of the number of *f*-electrons to the total requires highly accurate intensity measurement. Third, in crystals with heavy atoms absorption, extinction and MD affect the measured intensities severely.

Several papers on the *f*-electron density have been reported. That for CeB_6 at 298 and 100 K was measured by Sato (1985). Refinement of the data at 100 K converged to a final *R* value of 0.003 and significant peaks 0.3 e Å^{-3} high were found on the deformation density map along ⟨100⟩ directions displaced 0.4 Å from Ce. The *f*-electron densities of La, Ce, Pr, Nd, Sm, Eu, Gd, Tb, Dy, Yb and Lu in a series of nonaaqualanthanoid(III) tris(trifluoromethane)sulfonates were measured by Chatterjee, Maslen & Watson (1988). Significant peaks were found around the lanthanoid atoms, which show a trend of strengthening with increasing lanthanoid atomic numbers. However, in these earlier works the aspherical features were not analyzed quantitatively with scattering factors that take the aspherical *f*-electron density distribution into account. Therefore, the aspherical features have not been confirmed as being due to 4*f*-electrons.

The typical dense Kondo material cerium hexaboride, CeB_6, has been extensively studied. It is paramagnetic down to the quadrupolar ordering temperature $T_Q = 3.2$ K (Fujita, Suzuki, Komatsubara, Kunii, Kasuya & Ohtsuka, 1980) and again undergoes magnetic ordering transitions at the Néel temperature $T_N = 2.2$ K (Kasuya, Takegahara, Aoki, Suzuki, Kunii, Sera, Sato, Fujita, Goto, Tamaki & Komatsubara, 1982). Above T_Q the electrical resistivity exhibits a

$-\log T$ dependence with the Kondo temperature $T_K = 2$ K. The sixfold degenerate ground state of Ce^{3+} ($J = 5/2$) splits into a Γ_7 doublet and Γ_8 quartet. Γ_8 was established to be the ground state by inelastic magnetic neutron scattering (Zirngiebl, Hillerbrands, Blumenröder, Güntherodt, Loewenhaupt, Carpenter, Winzer & Fisk, 1984) and by the measurement of the magnetization process (Sato, Kunii, Oguro, Komatsuzawa & Kasuya, 1984). The Fermi surface for CeB_6 was determined by measuring the angle dependence of the de Haas–van Alphen frequency and the field-dependence of the heavy cyclotron mass was also determined (Ōnuki, Komatsubara, Reinders & Springford, 1989).

The space group of CeB_6 is $Pm\bar{3}m$. The Ce atom is at the body-centered position in the O_h crystal field formed by the regular B_6 octahedra at corners with each B atom on an edge. The following discussion in the present article assumes B at $(0, 0, z)$. Since the Ce^{3+} $4f$-orbitals are shielded by fully occupied $5s$- and $5p$-shells, the crystal field splitting is expected to be much smaller than splitting by spin-orbit interaction. Since Ce^{3+} has one $4f$-electron, its atomic ground state forms a regular sextet structure and it has a total angular momentum quantum number $J = 5/2$, in which the orbital angular momentum ($L = 3$) is antiparallel to the spin ($S = 1/2$). In the O_h crystal field it further splits into Γ_7 and Γ_8, with the state $J = 7/2$ splitting into Γ_6, Γ_7 and Γ_8 states. Neglecting the spin-orbit interaction, the seven f-orbitals in the O_h crystal field split into two sets of triply degenerate orbitals, $t_{1u}\{5x^3 - 3xr^2,\ 5y^3 - 3yr^2,\ 5z^3 - 3zr^2\}$ and $t_{2u}\{x(y^2 - z^2),\ y(z^2 - x^2),\ z(x^2 - y^2)\}$, and an orbital $a_{2u}\{xyz\}$ arranged in order of increasing energy. Since these orbitals are clearly defined within the limit of the crystal field theory, scattering factors for electrons in these orbitals can be evaluated with no ambiguity. By spin-orbit interaction T_{1u} splits into Γ_6 and Γ_8, T_{2u} into Γ_7 and Γ_8, and A_{2u} reduces to Γ_7 in the O_h crystal field. Thus, the ground state Γ_8 can be correlated to T_{1u} or T_{2u}. The present article aims to measure f-electron density distribution in CeB_6 crystals and identify it as due to f-electrons either on the t_{1u}- or t_{2u}-orbital. We denote this analysis utilizing the aspherical scattering factors, which are calculated based on the individual AO, and keeping the orthonormal relationships between AO's as X-ray AO analysis.

By the X-ray AO analysis we have studied d-electron densities in transition metal complexes. Hybridized orbitals in $KCuF_3$ (Tanaka, Konishi & Marumo, 1979) and $CuAlO_2$ (Ishiguro, Ishizawa, Mizutani, Kato, Tanaka & Marumo, 1983) were determined, keeping orthonormal relationships between the d-orbitals and between the $3d$- and $4s$-orbitals, respectively. Measurements of the electron densities in KMF_3 (M = Mn, Fe, Co) indicated definitively that the metals have the high-spin configuration (Kijima, Tanaka & Marumo, 1982, 1983; Miyata, Tanaka & Marumo, 1983). Recently, $3d$-orbitals for Cu^{2+} in $[Cu(diazacyclooctane)_2](NO_3)_2$, located at a C_i site in crystals, were determined (Tanaka, 1993) with the least-squares method incorporating orthonormal relationships between d-orbitals (Tanaka, 1988). These earlier papers analyzed only the electron densities around the transition metals. In the present article $2s$-, $2p_x$-, $2p_y$- and $2p_z$-electrons for B as well as the Ce f-electrons are treated with the aspherical scattering factors, keeping the crystal electrostatistically neutral.

2. Experimental

Crystals of CeB_6 were grown by the floating zone method. In the X-ray electron density study by Sato (1985) the residual electron density revealed a large trough on the B-atom sites, indicating 3 (100 K) to 7% (298 K) deficiency of the B atoms. The crystal used in the present study has no such deficiency. Since the total number of electrons in the unit cell is 88 and there is only one $4f$-electron if the formal valence of +3 for Ce is assumed, highly accurate measurement of structure factors is necessary. The crystal specimen was, therefore, shaped into a sphere with diameter 72 μm by the modified Bond method (Bond, 1951; Tsuchida, Kato, Tanaka & Marumo, 1990). The diameter was measured by taking photographs of the specimen with a scale of 2 μm units multiplied by 400 times under a microscope. This is the smallest spherical specimen used in our accurate measurements of structure factors. The lattice parameters were calculated from 2θ values for a total of 50 reflections, {155}, {633}, 444 and $\bar{4}\bar{4}\bar{4}$ with 2θ greater than 70°. The smaller the crystal, the less pronounced the systematic errors due to absorption, extinction and MD. As MD occurs frequently and its intensity perturbation is very significant for crystals containing heavy atoms, it was avoided using the ψ-scan method (Tanaka, Kumazawa, Tsubokawa, Maruno & Shirotani, 1994). There were more than one secondary reflection for every ψ. Fluctuations δF of structure factors F, induced by one secondary reflection, which fulfills the reflection condition simultaneously with the primary one, were calculated for each ψ from 0 to 359° at intervals of 1°. When the largest fluctuation $\delta F/F$ was less than 0.003 for the primary reflections with $2\theta < 90°$, 0.005 for those with $90 < 2\theta < 120°$ and 0.007 for those with $120 < 2\theta < 150°$, structure factors of primary reflections were measured. Structure factors were measured at 165 K on a four-circle diffractometer (MXC3; MAC Science) equipped with an Oxford Cryostream Cooler (Oxford Cryostreams; Cosier & Glazer, 1986). The diffractometer was installed in a box covered with a vinyl sheet filled with nitrogen gas to prevent ice forming on the crystal. When the intensities of reference reflections fluctuated significantly due to the ice formation, ice was blown off using a room-temperature nitrogen gas stream through a tube inserted

in the box. However, nitrogen gas flow was used only a few times during the 14 d measurement. The cryostat was fixed on a plate which permitted small translation along x, y and z directions, and rotations around the x and z axes (Kato, 1994). When the temperature at the sample position was measured by mounting a copper–constantan thermocouple on a goniometer, significant temperature fluctuations for rotations of the ω and χ angles were observed. The majority of reflections were measured avoiding MD in *region* 0 below the line $\chi = -0.505\omega$ for $\omega < 0°$ and $\chi = 0.2\omega$ for $\omega \geq 0°$ and above the lines $\chi = 0.4\omega - 37°$ for $\omega < 30°$ and $\chi = -25.0°$ for $\omega \geq 30°$, where temperature fluctuation is less than 1°. Reflections remaining outside the region were measured expanding the region by 10° three times for both lower and upper χ angles (*regions* 1–3). The temperature fluctuations in *regions* 1, 2 and 3 were approximately 1, 2 and 5°, respectively. Reflections with $0 < 2\theta \leq 30°$ and {310}, {311}, {321} and {400} were measured in full reciprocal space so as to apply the anisotropic extinction correction reliably. The other reflections with 2θ up to 150° were measured in an octant. If a reflection in an octant could not be measured avoiding MD in *regions* 0–3, proper equivalent reflections in other octants that did not involve permuting the Miller indices were measured. In *regions* 0–3 578, 155, 76 and 49 reflections, respectively, were measured. The number of independent reflections is 187 compared with a total number with 2θ less than 150° of 193. Six independent reflections could not be measured in *regions* 0–3 avoiding MD. The full experimental conditions and the crystal data are summarized in Table 1. The four angles 2θ, ω, χ and φ for each reflection were recorded on a file for the following refinements.

Table 1. *Crystal data of CeB_6 at 165 K and experimental conditions*

Space group	$Pm\bar{3}m$
Z	1
a (Å)	4.13814 (4)
V (Å^3)	70.863 (2)
D_x (g cm^{-3})	4.80330
Formula weight	204.981
Wavelength (Mo $K\alpha$, Å)	0.71069
μ (Mo $K\alpha$, mm^{-1})	15.996
Crystal diameter (μm)	72
Scan type	ω–2θ
Scan speed in ω (° min^{-1})	2
Number of scans	10
$2\theta_{max}$ (°)	150
Number of reflections	
Measured	875
Used	844
Independent	187

3. Refinement

3.1. *Refinement with spherical scattering factors*

The ionic model, Ce^{3+} and B_6^{3-}, was assumed at the initial stage of refinement. In order for the electron density around each atom to be spherical, 1/7 electrons were allotted to each of seven basis f-orbitals for Ce^{3+}. Since the six B atoms in B_6 are equivalent by symmetry, the valence state $-1/2$ was assumed for each B atom. The configuration $1s^2 2s^2 2p_x^{1/2} 2p_y^{1/2} 2p_z^{1/2}$ was thus assumed for B. Since the AO's for Ce are highly relativistic, they were calculated by the Dirac–Slater method using the program *HEX* by Liberman, Cromer & Waber (1971). The scattering factors f_{AO} were calculated from Ce 1s- to 4f-radial functions. Derivatives of f_{AO} with respect to the distance r from the nucleus, df_{AO}/dr, and $\langle j_n(kr)\rangle$, the average of the spherical Bessel functions of the order n (= 0,2,4,6), were also calculated using the program *AO2SF* coded by one of the authors (KT). df_{AO}/dr is required to refine the expansion and contraction parameter κ of each AO described in the following section. Atomic scattering factors for B are based on the Hartree–Fock AO's (Mann, 1968) and anomalous dispersion terms for Ce and B were from *International Tables for X-ray Crystallography* (1974, Vol. IV). Equal weights (= 1) were assigned to reflections measured in *regions* 0–3 described in the previous section. After refinement using spherical scattering factors assuming Type I extinction with the Thornley–Nelmes distribution function (Thornley & Nelmes, 1974) reduced the R and wR factors to 0.016 and 0.017, respectively. $y_{min}(= F_o/F_c)$ was 0.628 for $\bar{1}10$.

3.2. *X-ray AO analysis*

Assuming a point charge of -0.5 e on each B atom, the crystal field splitting for the seven f-states was calculated following the method given by Kamimura, Sugano & Tanabe (1969). Scattering factors of f-electrons in the O_h crystal field were derived by Weiss & Freeman (1959). In the present study the quantization axes x, y and z for Ce and B were taken parallel to the crystal axes a, b and c, respectively. The ith 4f-orbital ψ_i is expressed in terms of the seven mutually orthogonal f-orbitals, φ_k, which are identical to t_{1u}, t_{2u} and a_{2u} orbitals described in the foregoing section, in the following way,

$$\psi_i = \Sigma c_{ik}\varphi_k(\kappa_i r),$$

where κ_i expresses the expansion ($\kappa_i < 1$) or contraction ($\kappa_i > 1$) of the ith f-orbital in the crystal. The parameter κ was first introduced by Coppens, Guru Row, Leung, Stevens, Becker & Yang (1979) to express the contraction and expansion of the whole valence electron densities. In the present X-ray AO analysis κ_i assigned to each f-orbital, not to the valence electron densities, obeying the crystal symmetry so that κ_i for degenerate orbitals are identical (Tanaka, 1988). For orbitals in an O_h symmetry field the crystal field theory indicates that the coefficients $c_{ii} = 1$; the remainder are zero.

Consequently, κ_i and the population of electrons, n_i, of the orbitals for Ce and B as well as the atomic parameters were determined in the following refinement. Since B is on a fourfold axis, the p_x- and p_y-orbitals are equivalent. Populations and κ values for B $2p_x$ and $2p_y$ are restricted to be equal, while those for $2p_z$ can be shifted independently.

Electron populations for Ce t_{1u}, t_{2u} and a_{2u} were varied together with those for B $2s$ and $2p$, keeping the crystal electrostatistically neutral. Since the populations for Ce a_{2u} and B $2s$ always became negative and exceeded 2, respectively, they were fixed at 0 and 2. A negative Ce a_{2u} population indicates that no electrons locate in the orbital. A fully occupied B $2s$-orbital will be discussed in the next section. Since the population of Ce t_{2u} tended towards zero at the initial stage of refinement, but did not vanish completely, two models were tested. The first assumed that the ground state for Ce^{3+} was t_{1u} and an electron occupied the three t_{1u} orbitals equally. The second assumed that electrons were both on t_{1u} and t_{2u} and the parameters for both orbitals were refined. The populations n of t_{1u} and t_{2u} after the second refinement converged to $n(t_{1u}) = 0.68\,(9)$ and $n(t_{2u}) = 0.22\,(26)$. The population on t_{2u} is less than its error in parentheses. Thus, it was judged to be insignificant and all further refinements were based on the first model.

3.3. *Anharmonic thermal vibration analysis*

Since anharmonic thermal vibration is another source of aspherical electron density distribution and since $4f$-orbitals locate closer to a nucleus and are expected to be affected strongly by thermal vibration, that for Ce as well as for B was analyzed after the X-ray AO analysis using the method by Tanaka & Marumo (1983), which made possible general use of the method by Dawson, Hurley & Maslen (1967). Anharmonic cubic and quartic parameters were used for B at the site with the point-group symmetry $4mm$. Quartic parameters were used for Ce at the site with $m\bar{3}m$ point-group symmetry. Anharmonic potentials V_a for Ce at (1/2,1/2,1/2) and B at (0,0,z) are expressed as

$$V_{a,\mathrm{Ce}} = q_{1111}(u_1^4 + u_2^4 + u_3^4) + q_{1122}(u_1^2u_2^2 + u_1^2u_3^2 + u_2^2u_3^2),$$

$$V_{a,\mathrm{B}} = c_{111}(u_1^3 + u_2^3) + c_{333}u_3^3 + q_{1111}(u_1^4 + u_2^4) + q_{3333}u_3^4 + q_{1122}u_1^2u_2^2 + q_{1133}(u_1^2u_3^2 + u_2^2u_3^2),$$

where (u_1, u_2, u_3) is a displacement vector from the equilibrium position of each atom. Cartesian coordinates for the displacement vectors are parallel to the lattice axes. The anharmonic parameters were refined fixing the harmonic temperature factors. The anharmonic cubic parameters of B were refined with the z coordinate, resulting in a significant shift. The interactions between the parameters in each pair q_{1111} and q_{1122}, q_{1133} and q_{3333} of B, and q_{1111} and q_{1122} of Ce were severe and the parameters in each pair were refined separately. The refinement in §3.3 was carried out after the refinement in §3.2. All the anharmonic parameters were insignificant, except for c_{333} of B.

4. Result and discussion

4.1. *4f-electron density distribution of the Ce atom*

The atomic and extinction parameters after the refinements in §3.1–3.3* are listed in Tables 2(*a*) and (*b*), respectively, together with R and wR factors. The deformation densities around Ce after the refinement in §3.1 are illustrated in Fig. 1. There are large peaks with height $2.0\,\mathrm{e\,\AA^{-3}}$ at 0.41 Å from Ce^{3+} along ⟨100⟩ directions. Peaks due to $3d$-electrons have usually been found at ~0.5 Å from the nucleus. Since $4f$-electrons are closer to the nucleus than $3d$-electrons, these peaks were expected to be those for the aspherical electron density distribution of Ce $4f$-electrons. In a previous electron density study on CeB_6 by Sato (1985), similar peaks with height $0.3\,\mathrm{e\,\AA^{-3}}$ were found around the Ce atom at 100 K and were attributed to the electrons in the Γ_8 ground state.

Refinements of orbital parameters reduced R and wR factors significantly to 0.0075 and 0.0090, respectively. Refinement of anharmonic vibration parameters

* A list of structure factors has been deposited with the IUCr (Reference: OA0003). Copies may be obtained through The Managing Editor, International Union of Crystallography, 5 Abbey Square, Chester CH1 2HU, England.

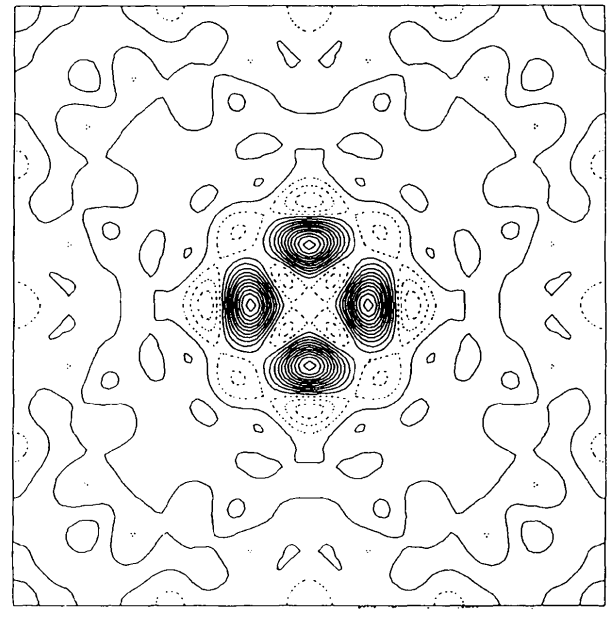

Fig. 1. Deformation density after the refinement in §3.1 around Ce at $(\frac{1}{2},\frac{1}{2},\frac{1}{2})$ on the plane (001) in the region $0 \le x, y \le 1$. Contours are at intervals $0.2\,\mathrm{e\,\AA^{-3}}$; zero and positive contours as full lines and negative contours as broken lines.

Table 2. *Extinction and final parameters*

(*a*) Parameters for B at (0, 0, *z*). Fractional coordinates ($\times 10^{-4}$), populations n ($\times 10^{-2}$), κ ($\times 10^{-2}$), anisotropic temperature factors U^{ij} ($\times 10^{-5}$ Å^2), anharmonic cubic parameters c_{ijk} ($\times 10^{-20}$ J Å^{-3}), quartic parameters q_{iijj} ($\times 10^{-20}$ J Å^{-4}). Anisotropic temperature factors are defined as $T_H = \exp[-2\pi^2 \Sigma_{ij} h_i h_j a_i^* a_j^* U^{ij}$ and anharmonic potentials V_a are defined in the text.

	§3.1	§3.2	§3.3
Ce			
U^{11}	374 (3)	344 (4)	345 (1)
n (T_{1u})		84 (8)	83 (8)
κ (T_{1u})		172 (9)	172 (9)
q_{1111}			1 (6)
q_{1122}			−5 (17)
B			
z	3009 (2)	3009 (2)	2973 (5)
U^{11}	414 (11)	388 (12)	388 (12)
U^{33}	318 (17)	242 (19)	252 (21)
n (2s)		200	200
n (2p_x)		39 (4)	39 (4)
n (2p_z)		47 (8)	47 (8)
κ (2s)		95 (4)	95 (4)
κ (2p_x)		96 (13)	96 (13)
κ (2p_z)		115 (8)	115 (8)
c_{311}			−21 (65)
c_{333}			−174 (82)
q_{1111}			21 (62)
q_{3333}			−47 (369)
q_{1122}			38 (374)
q_{1133}			−270 (375)
R	0.016	0.0075	0.0075
wR	0.017	0.0090	0.0090

(*b*) Anisotropic type I extinction parameters with Thornley-Nelmes distribution function

Y_{11}	67 (4)	88 (7)	88 (7)
Y_{22}	168 (7)	229 (17)	229 (17)
Y_{33}	38 (1)	47 (3)	47 (3)
Y_{12}	84 (5)	107 (9)	107 (9)
Y_{13}	−21 (2)	−27 (3)	−27 (3)
Y_{23}	−45 (2)	−63 (5)	−63 (5)

reduced R and wR factors only slightly. However, z for B shifted only after refinement of the anharmonic parameters. The effect of the anharmonic cubic parameters on the deformation density will be discussed in the following section. In the deformation density after the refinement in §3.3, illustrated in Fig. 2, the large peaks in Fig. 1 are not found. This indicates clearly that the large peaks in Fig. 1 are those for the 4*f*-electrons in the T_{1u} state. The present study, to our knowledge, is the first in which the 4*f*-electrons are analyzed quantitatively based on a proper quantum mechanical model, taking into account the aspherical 4*f*-electron density distribution. The electron population in Ce T_{1u} is 0.83 (8), indicating that the charge on the Ce atom is +1.5 (2) e. This value is much smaller than the formal charge +3 e, which corresponds to the population 1/3 e in each of the three t_{1u}-orbitals, indicating significant donation of electrons from B_6 to Ce. The alternative X-ray AO analysis, keeping the formal charge of Ce, reduced the peak height of the large peaks in Fig. 1 to half and the anharmonic temperature factors for Ce and B were significant. However, the peaks along ⟨100⟩ directions with height 0.6 e Å^{-3} remained even after refinement of the anharmonic thermal vibration. In order to see the effect of the anharmonic thermal vibration on deformation densities, the intensities are being remeasured at 100, 230 and 298 K. The results will be reported elsewhere. The κ parameter 1.72 (9) for Ce t_{1u} indicates that these orbitals are strongly contacted in the crystal. In other words, the energy of the 4*f*-state or that of the band composed mainly of the 4*f*-orbitals is lowered since the orbital for the state locates closer to the nucleus.

Since the troughs around the Ce atom in Fig. 2 with the depth −0.6 e Å^{-3} along ⟨100⟩ directions and those with depth −0.2 e Å^{-3} along ⟨110⟩ directions seem to be significant, possible origins of these troughs were investigated. The structure factors were calculated excluding a part of the contribution of Ce 5*p*-electrons. The troughs were gradually diminished with a decrease in the contribution of Ce 5*p*-electrons to the structure factors. When four Ce 5*p*-electrons with $j = 3/2$ were not involved in the structure-factor calculation, both troughs along ⟨100⟩ and ⟨110⟩ were transformed into peaks with heights 0.6 e Å^{-3}, although a very large peak of 2.6 e Å^{-3} at the Ce atomic position newly appeared. The difference density is illustrated in Fig. 3. Therefore, the troughs around Ce in Fig. 2 are correlated to Ce 5*p*-electrons. However, a simple model modifying the 5*p*-population under the constraint of electroneutrality produced more residual density on the Ce atomic position and refinement did not reduce the R factors. Hybridized orbitals between 4*f*- and 5*p*-orbitals, having

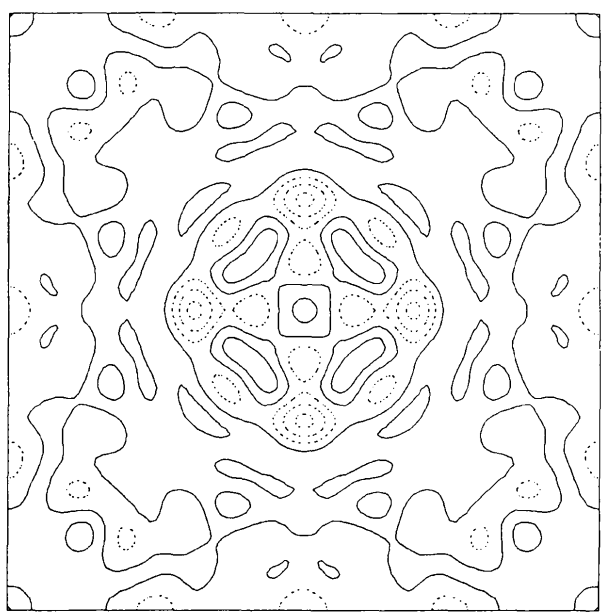

Fig. 2. Deformation density around Ce after the refinement in §3.3. Contours are as in Fig. 1.

a centrosymmetric configuration that conforms with the point-group symmetry for Ce, may possibly explain these troughs. The large κ value for the 4*f*-orbitals seems to be explained by this model, which will be tested further and published elsewhere.

4.2. *Electron density around the B_6 molecule and their anharmonic thermal vibration*

Peaks and troughs around the B atom on deformation density maps were examined to assess the quality of the present intensity measurement and analyses, although they are not as significant as those around Ce. The deformation density around the B_4 square on the (001) plane after the refinement in §3.1 is shown in Fig. 4. The center of the square is the origin of the lattice. Note that the contour interval $0.05\,e\,Å^{-3}$ is one fourth of those in Figs. 1–3. There are large peaks at the midpoints of the shortest B—B bonds connecting octahedra. At the midpoints of the B—B bonds in each octahedron there are peaks just outside the B_4 square. These peaks demonstrate the covalency of the B—B bonds. The peak $0.45\,e\,Å^{-3}$ at the origin is characteristic of the multi-centered bonds in borides. The characteristics of these peaks coincide qualitatively with the model deformation density map for CaB_6 (Ito & Higashi, 1986) composed only of light atoms. However, the peak with height $0.35\,e\,Å^{-3}$ on the B atomic position and the troughs with depths -0.65 and $-0.30\,e\,Å^{-3}$ at both sides in Fig. 4 are not found in CaB_6. These peaks found in CeB_6, but not found in CaB_6, cannot be explained by the present theories of chemical bonds. The peak at the origin has a peculiar shape. Peaks $0.15\,e\,Å^{-3}$ high also occur on the line between B and the origin. The $0.10\,e\,Å^{-3}$ peak between B and the middle of the B—B bonds connecting two octahedra is also strange, although these peaks are also found in CaB_6.

The deformation density after the refinement in §3.2 is illustrated in Fig. 5. X-ray AO analysis permitting electron donation from B_6 to Ce reduced the large peaks and troughs near B in Fig. 4. The peaks at the origin became smaller and more spherical. Those on the line joining B and the origin disappeared. However, a significantly high peak on the atomic site of B remained and was elongated toward the origin; the peak between B and the center of the B—B bonds connecting the two octahedra also persists. Moreover, all the peaks due to bonding electrons in the B—B bonds remained almost unchanged. These facts indicate that a simple AO model cannot describe the electron density in the B_6 molecule where the delocalized electrons cannot be neglected, while *d*- and *f*-electrons around transition metals are localized so much that they can be analyzed with AO models. In order to treat these delocalized densities, polarization functions used in MO calculations and multipole refinements are at least necessary and further analysis based on a MO model with the idempotency constraint should be investigated (Clinton, Frishberg, Massa & Oldfeld, 1973; Tanaka, 1988). Populations of $2s$, $2p_x = 2p_y$ and $2p_z$ for B in Table 2(*a*) are 2.0, 0.39(4) and 0.47(8), respectively. Their κ values are 0.95(4), 0.96(13) and 1.15(8), respectively. Resultant populations in the 2*p*-orbitals as well as the κ values are

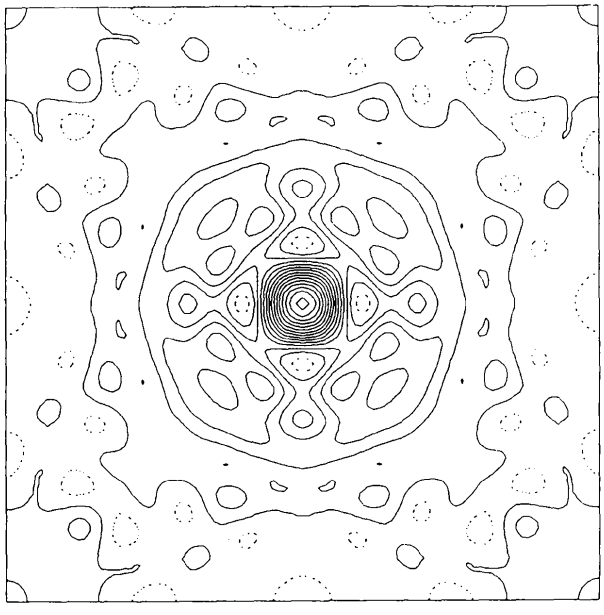

Fig. 3. Deformation density calculated after the refinement in §3.3 by deleting the four Ce 5*p*-electrons in the calculation of structure factors. Contours are as in Fig. 1.

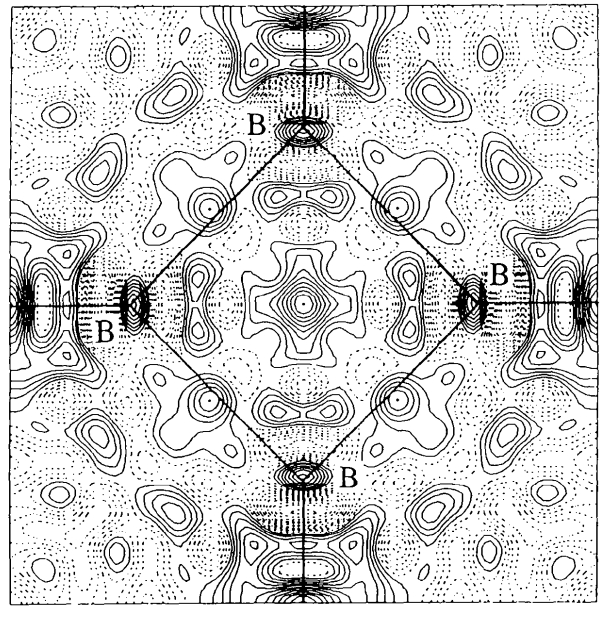

Fig. 4. Deformation density around the B_4 square after refinement in §3.2 in the region $-0.5 \le x, y \le 0.5$. Contours are as in Fig. 1, except the intervals are at $0.05\,e\,Å^{-3}$.

equal within experimental error. As pointed out by Dawson (1964), equally populated p_x, p_y and p_z state densities are spherical and almost identical to those of s state, which makes the partition of populations among $2s$ and the three $2p$-orbitals ambiguous. This is another reason for the failure of the present simple AO model to explain bonding electron density around the B atom and the reason for the fully occupied $2s$-orbital. The total amount of electrons in B_6, on the other hand, is reliable, since the deformation density around Ce was clearly explained and the large peaks and troughs around B in Fig. 4 disappeared in the refinement in §3.2, which allowed donation of electrons B_6 to Ce. Therefore, the deformation densities around B_6 calculated after the refinements in §3.2 and 3.3 are considered to be similar to those derived from a spherical atom model, although the B atoms in the present study are less populated than a neutral B atom. They demonstrate the features of delocalized electron density distribution in CeB_6, which include coordinate bonds between Ce and B_6.

The refinement in §3.1 revealed that the anharmonic cubic potential parameter c_{333} for B was significant (see Table 2*a*). Refinement of anharmonic thermal motion also shifted the B atoms along the z axis from $z = 0.3009(2)$ to $z = 0.2973(5)$ by a distance of 0.015 Å. Consequently, the B—B bond length between the octahedra increased from 1.6473(1) to 1.6775(2) Å and that in the octahedron reduced from 1.7613(2) to 1.7400(3) Å. The Ce—B distance increases from 3.03982(6) to 3.0439(2) Å. Fig. 6 shows the deformation density after the refinement in §3.3. All the peaks for the bonding electrons are linked continuously by positive electron density in Fig. 6. Neighboring octahedra are linked by continuous electron density elongated along the ⟨100⟩ directions. The significant peak on the B atom in Fig. 6 is elongated toward the center of the octahedron, even though B shifts toward the origin, which coincides with the direction of the main lobes of the bonding MO calculated by Longuet-Higgins & Roberts (1954), which will be discussed in the next paragraph. Since Cartesian coordinates for the displacement vectors were defined to be parallel to the lattice axes, negative c_{333} of the B atom indicates that its anharmonic vibration is favorable toward the shortest and thus the strongest B—B bond-adjoining octahedra. The direction is opposite to that toward the origin. This explains why the $0.10\,e\,Å^{-3}$ peak between B and the middle of the B—B bonds in Fig. 5 disappeared after the refinement in §3.3, see Fig. 6, although the effect of anharmonic vibrations on deformation density is minor compared with that of the donation of electrons from B to Ce. The deformation density in Fig. 6 is thus concluded to be closer to the real aspherical density distribution than Figs. 4 and 5. For $KCuF_3$ aspherical electron density due to anharmonic thermal vibration was revealed after the aspherical electron configuration due to the Jahn–Teller effect was removed (Tanaka & Marumo, 1982). The present analysis of the electron donation from B_6 to Ce and the anharmonic thermal vibration of B revealed an elongation of the electron density of B toward the origin, which characterizes the bonding MO for B_6.

Neglecting covalent metal–boron bonds, the electronic structure of the metal borides MB_6 was studied by

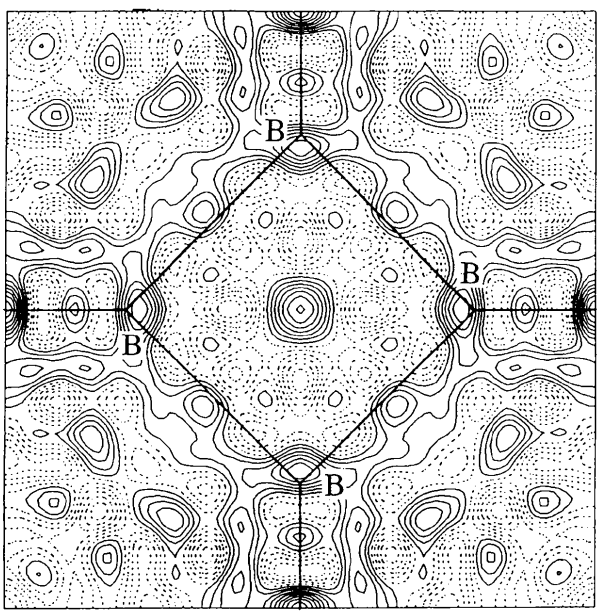

Fig. 5. Deformation density around B_4 after the refinement in §3.2. Contours are as in Fig. 4.

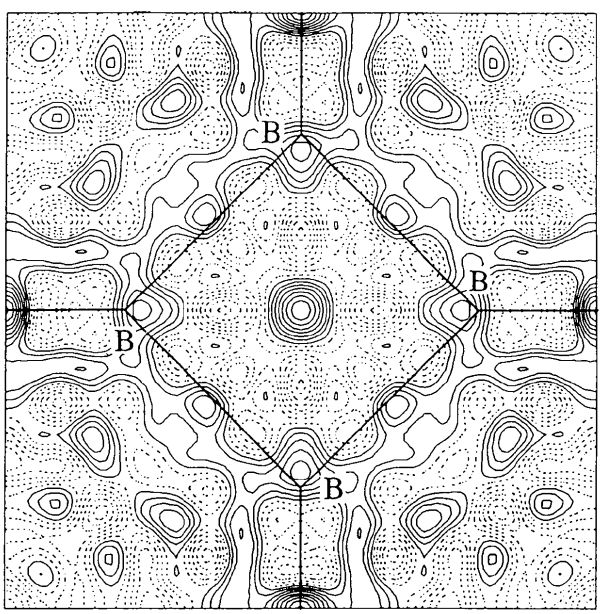

Fig. 6. Deformation density around B_4 after the refinement in §3.3. Contours are as in Fig. 4.

Longuet-Higgins & Roberts (1954) with what we can now term the extended Hückel method, although the evaluation of Coulomb and exchange integrals is different. Crystal orbitals were also constructed (Bloch, 1928) and the energy bands were presented. The bonding bands in increasing order of energy are E, A, F and B, according to their notation, accommodating 2, 6, 6 and 6 electrons, respectively. If the charge of the metal is +3, each B_6^{3-} unit has 21 bonding electrons. Longuet-Higgins & Roberts (1954) expected that the extra electron was largely associated with the unfilled 4*f*-orbitals on the metal atoms with the crystals acting as metallic conductors. The bonding MO for B_6 are illustrated schematically in Fig. 7. Each MO is expressed as a linear combination of the 2*s*- and 2*p*-basis functions of the B atoms in the B_6 moiety. Band E is an assembly of the a_{1g} basis orbital composed of 2*s*- and 2*p*-orbitals along the ⟨100⟩ directions. The lobes of a_{1g} point toward the center of the octahedron. Triply degenerate t_{1u} and t_{2g} are the components of bands A and B, respectively. The largest lobe of t_{1u} also points inward toward the origin. Therefore, the lowest two bands E and A explain why the peaks around the B atom in Fig. 6 are elongated toward the origin. The smaller lobes in t_{1u} and t_{2g} as well as those in t''_{1u} create the B—B bonds in each octahedron. Therefore, the bonding bands A and B correspond clearly to the deformation density around the B_4 square in Fig. 6. The orbitals a'_{1g}, t''_{1u} and e'_g contribute to band F. These three orbitals have the largest lobes extending outside the octahedron along the line connecting the origin to the B atom. These orbitals also mainly contribute to the formation of bonds between the octahedra. Accordingly, the calculated bonding MO corresponds very well to the deformation density in Fig. 6, which guarantees the quality of the present charge density measurement and makes detailed discussion of the deformation densities possible.

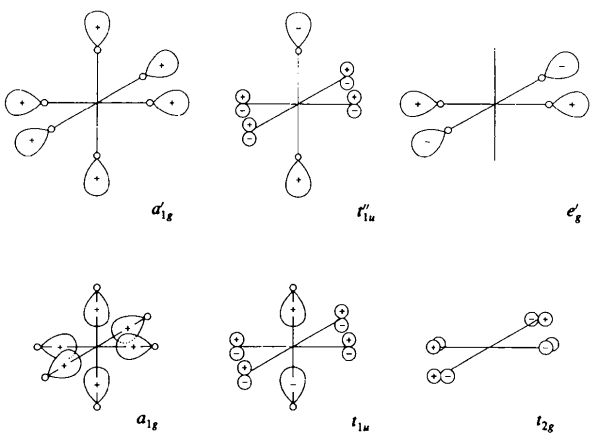

Fig. 7. Bonding MO of B_6 illustrated by Longuet-Higgins & Roberts (1954).

4.3. *Charge on each orbital and the Kondo effect*

The Kondo effect of CeB_6 is due to the partial cancellation of Ce 4*f*-spin by an admixture of conduction electrons with localized 4*f*-electrons. How the localized spin on Ce, however, is partially cancelled by the formation of hybridized orbitals is not clear. The electronic structures of rare-earth complexes are rather complicated, because of the coexistence of dominant spin-orbit interactions and crystal field splitting. The effect of the latter on the Kondo effect has been neglected. In order to investigate further the Kondo effect in CeB_6 by the X-ray diffraction method, analysis of the troughs around Ce should be carried out first so that the electronic structure of Ce is explained at least on the basis of an AO model. Further analyses of electron density which assume a MO model, including the Ce 4*f*-orbitals, may help solve the problem. However, the contribution of scattering factors of the two-center electrons between orbitals of metals and ligands, which characterize MO models for transition metal complexes, to structure factors is so small (Tanaka, 1996) that the X-ray MO analysis of CeB_6 may not give fruitful results with the present accuracy of X-ray intensity measurements. The present X-ray diffraction method may be accurate enough to carry out the X-ray MO analysis of B_6 in CeB_6, which neglect the interactions between Ce and B_6. This will help us determine the electron distribution around B_6 and areas between Ce and B_6.

However, the present study revealed two points, which can be correlated to the Kondo effect. First, the large κ value 1.72 (9) in Table 2(*a*) of the 4*f*-orbitals in the present study implies that the 4*f*-orbitals are stabilized because they are located closer to the positive Ce nucleus. The energy of the 4*f*-orbital relative to the Fermi level is an important factor affecting the degree of hybridization and the Kondo effect. Second, the electron population of Ce t_{1u} is 0.83 (8) in Table 2(*a*), resulting in the net charge +1.5 (2) e on Ce. This is as predicted by Longuet-Higgins & Roberts (1954). The 4*f*-orbital population may reflect the degree of delocalization of electrons due to hybridization. Since the Kondo effect in CeB_6 occurs over temperatures ranging from extremely low to above room temperature, further experiments at several temperatures followed by analysis of the temperature dependence of electron densities would help clarify the origin of the Kondo effect. Intensity measurement at 100, 230 and 298 K have commenced. The results will be published elsewhere.

CeB_6 is a metallic conductor and 1.5 (2) e are donated from B_6 to Ce at 165 K. Band theory assumes conduction bands extending throughout metals and energy bands have been calculated. However, since band theory is based on Bloch functions for a periodic

potential and not on orbital models such as AO and MO, spatial overlapping of orbitals and distribution of conduction electrons in metals have not been considered seriously. It is worthwhile to examine, based on MO models, if there are paths for the electron donation, although X-ray diffraction is probably not accurate enough at present to treat two-center electron density between Ce and B_6. If electrons jump from B_6 to Ce in a very short time, no electron density is expected to be observed between B_6 and Ce. However, if a MO is formed, a significant amount of electrons is expected to exist stationary between B_6 and Ce, and the electron density may be seen. Among the overlap integrals calculated for orbitals joining adjacent octahedra, those between the t''_{1u} orbitals are the largest, followed by those between e'_g and a'_{1g}, which comprise band F (Longuet-Higgins & Roberts, 1954). These accumulate at the midpoint of each edge of the lattice, which is also the midpoint of the B—B bonds adjoining the B_6 octahedra. That edge center is the closest to the body center where the Ce atom locates. Denoting one of the t''_{1u}-orbitals for the B_6 molecule with the main lobe along z as $t''_{1u,z}$, it is easily realized that the overlap integrals between $t''_{1u,z}$ and $f_{5z^3-3zr^2}$ do not vanish. Bonding MO of CeB_6 along z is expected to be a linear combination of Ce $f_{5z^3-3zr^2}$, and $t''_{1u,z}$- and $t_{1u,z}$-orbitals for B_6 with the main contribution from the $t''_{1u,z}$-orbital for B_6. The antibonding MO is composed mainly of Ce $4f$. The electrons on B_6 are, therefore, expected to be donated mainly through B_6 t''_{1u} to Ce t_{1u}. Both orbitals have main lobes extending along the ⟨100⟩ directions. The deformation density on the (110) plane is illustrated in Fig. 8, on which the main lobes of $t''_{1u,z}$ and $f_{5z^3-3zr^2}$ coexist. The edge center and the Ce atom are connected clearly by positive electron density, supporting the fact that one of the possible paths for electron donation is through the orbitals in the T_{1u} states.

This work was supported in part by a Grant-in-Aid for Scientific Research No. 05453021 and on Priority Area (nos. 07231212 and 07231212) from the Ministry of Education, Science and Culture.

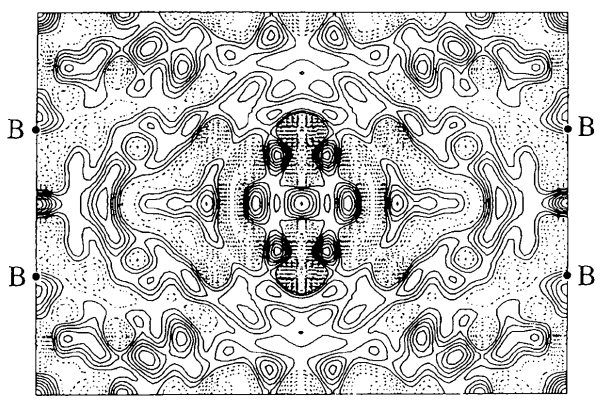

Fig. 8. Deformation density on (110), on which the main lobes of B_6 $t''_{1u,z}$ and Ce $f_{5z^3-3zr^2}$ coexist. Ce locates t the center of the figure. Contours are as in Fig. 4.

References

Bloch, F. (1928). *Z. Phys.* **52**, 555–600.

Bond, W. L. (1951). *Rev. Sci. Instrum.* **22**, 344.

Chatterjee, A., Maslen, E. N. & Watson, K. J. (1988). *Acta Cryst.* B**44**, 386–395.

Clinton, W. L., Frishberg, C. A., Massa, L. J. & Oldfeld, P. A. (1973). *Int. J. Quantum Chem. Symp.* **7**, 505–514.

Coppens, P., Guru Row, T. N., Leung, P., Stevens, E. D., Becker, P. J. & Yang, Y. W. (1979). *Acta Cryst.* A**35**, 63–72.

Cosier, J. & Glazer, A. M. (1986). *J. Appl. Cryst.* **19**, 105–107.

Dawson, B. (1964). *Acta Cryst.* **17**, 997–1009.

Dawson, B., Hurley, A. C. & Maslen, V. W. (1967). *Proc. R. Soc. London Ser. A*, **298**, 289–306.

Fujita, T., Suzuki, M., Komatsubara, T., Kunii, S., Kasuya, T. & Ohtsuka, T. (1980). *Solid State Commun.* **35**, 569–572.

Ishiguro, T., Ishizawas, B., Mizutani, N., Kato, M., Tanaka, K. & Marumo, F. (1982). *Acta Cryst.* B**39**, 564–569.

Ito, T. & Higashi, I. (1986). *Chem. Scr.* **26**, 479.

Kamimura, H., Sugano, S. & Tanabe, Y. (1969). *Ligand Field Theory and its Applications*. Tokyo: Syokabo.

Kasuya, T., Takegahara, Y., Aoki, T., Suzuki, T., Kunii, S., Sera, M., Sato, N., Fujita, T., Goto, T., Tamakii, A. & Komatsubara, T. (1982). *Proceedings of the International Conference on Valence Imstability*, edited by P. Wachter & H. Boppart, pp. 359–359. Amsterdam: North-Holland.

Kato, Y. (1994). Unpublished work.

Kijima, N., Tanaka, K. & Marumo, F. (1982). *Acta Cryst.* B**38**, 545–548.

Kijima, N., Tanaka, K. & Marumo, F. (1983). *Acta Cryst.* B**39**, 557–561.

Liberman, A., Cromer, D. T. & Waber, J. T. (1971). *Comp. Phys. Commun.* **2**, 107–113.

Longuet-Higgins, H. C. & Roberts, M. de V. (1954). *Proc. R. Soc. London Ser. A*, **224**, 336–347.

Mann, J. B. (1968). Report LA3691. Los Alamos, New Mexico, USA.

Miyata, N., Tanaka, K. & Marumo, F. (1983). *Acta Cryst.* B**39**, 561–564.

Ōnuki, Y., Komatsubara, T., Reinders, P. H. P. & Springford, M. (1989). *J. Phys. Soc. Jpn*, **58**, 3698–3704.

Sato, N., Kunii, S., Oguro, I., Komatsuzawa, T. & Kasuya, T. (1984). *J. Phys. Soc. Jpn*, **53**, 3967–3979.

Sato, S. (1985). *J. Magn. Magn. Mater.* **52**, 310–312.

Tanaka, K. (1988). *Acta Cryst.* A**35**, 1002–1008.

Tanaka, K. (1993). *Acta Cryst.* B**49**, 1001–1010.

Tanaka, K. (1996). *Mol. Cryst. Liq. Cryst.* **278**, 111–116.

Tanaka, K. & Marumo, F. (1982). *Acta Cryst.* A**38**, 1422–1427.

Tanaka, K. & Marumo, F. (1983). *Acta Cryst.* A**39**, 631–641.

Tanaka, K., Konishi, M. & Marumo, F. (1979). *Acta Cryst.* B**35**, 1303–1308.

Tanaka, K., Kumazawa, S., Tsubokawa, M., Maruno, S. & Shirotani, I. (1994). *Acta Cryst.* **A50**, 246–252.

Thornley, F. R. & Nelmes, R. J. (1974). *Acta Cryst.* **A30**, 748–757.

Tsuchida, T., Kato, M., Tanaka, K. & Marumo, F. (1990). Unpublished work.

Weiss, R. J. & Freeman, A. J. (1959). *J. Phys. Chem. Solids,* **10**, 147–161.

Zirngiebl, E., Hillerbrands, B., Blumenröder, S., Güntherodt, G., Loewenhaupt, M., Carpenter, J. M., Winzer, K. & Fisk, Z. (1984). *Phys Rev. B*, **30**, 4052–4054.